International Journal of Dynamics of Fluids.
ISSN 0973-1784 Volume 19, Number 1 (2023), pp. 1-17

http://www.ripublication.com

Performance Assessment of a Nearshore Distensible-Tube Wave Attenuator at Model Scale

Antonio C. Mendes[1] and Francisco P. Braga[2]

Laboratory of Fluid Mechanics and Turbomachinery
Electromechanical Engineering Department
Universidade da Beira Interior, 6201-001 Covilha, Portugal
E-mail: [1]Corresponding author: acmendes@ubi.pt
[2]Contributing author: francisco.p.braga@ubi.pt

Abstract

A water-filled floating rubber tube is considered for ocean wave power absorption. Its working principle relies on wave-excited pressure bulges delivered by the tube into a forward-bent oscillating water column at its stern. The present study reports on wave flume tests conducted with a 1:70 scale model of this system, in deep and intermediate regular waves having small and finite amplitudes. An orifice-flow pneumatic power take-off is used to emulate an air turbine generator set. Assuming incompressible flow, its nonlinear pressure to volume-flow characteristic is here obtained from the water column free-surface measurements, for different wave loading conditions. Two situations are considered: the system operating over a sloping bottom nearshore or fitted into a sea-wall onshore. In this latter case the influence of water depth variation is also investigated. The hydrodynamic and overall efficiencies of the system are provided. It is demonstrated that the system is very efficient when the tube is allowed to operate with three degrees-of-freedom: in bending, surging and bulging modes. Additionally, it is shown that its performance is higher in the onshore configuration.

Keywords: Wave energy; Distensible tube; Wave-flume tests; Performance assessment.

1. Introduction

Estimates of the global gross wave energy potential advanced by the World Energy Council in 2016 [1] point to 32 000 TWh per year. However, it is generally assumed that the gross nearshore resource is much smaller than the corresponding gross wave

energy potential offshore, regardless of bathymetry. This is not always so, as the wave attenuation will be closely dependent on the continental shelf and the directionality of the waves. Sometimes there can even be a natural focussing effect that may be beneficial for wave energy harnessing. Apropos, Foley and Whittaker [2] argue that the gross wave power resource is not an appropriate measure. Instead they have introduced a rational quantification of the nearshore exploitable wave energy resource, which accounts for wave directionality and also for the rated power limit of the plant. From this point of view the wave energy resource will not be so dramatically reduced by refraction near the coast, because the directional spread of the waves tends to become smaller at the nearshore. In fact, for the typical wave climates of the mid and north Atlantic the reduction of net wave power density is expected to be well below 20% in seabed slopes of 1:100. If we accept this definition, the deployment of wave energy converters in the nearshore may become economically viable.

The purpose of the present research is to use a concept proposed by Farley and Rainey in 2006 [3] and adapt it to operate in the nearshore. It consists of a long floating rubber tube filled with water – The *Anaconda* – that can be utilized to efficiently harness the energy of ocean waves. An independent analysis done by the Carbon Trust in 2010 suggested that this concept had the potential to deliver significant reductions in the cost of wave energy. It could therefore belong to a future generation of profitable ocean renewable energy converters. The first laboratory tests of the *Anaconda* were carried out in 2007, with a model of this device having a $2.5\ m$ long latex tube, $0.078\ m$ in diameter and $0.15\ mm$ wall thickness [4]. The model was tested in a wave flume, submerged just below the still water level. The experiment provided evidence of a capture-width of 3 to 4 tube diameters in a wide range of incident wave frequencies. Since the device was not fitted with any power take-off system, the wave energy it absorbed was in this case accounted for by hysteresis losses in the rubber and friction losses of the internal flow. The working principle of the *Anaconda* wave power converter has been reanalysed and discussed in detail in [5]. Later, Chaplin et al. [6] performed in 2010 a second series of tests with a 1:25 scale model at the Offshore Wave Basin of the Danish Hydraulic Institute, in Denmark. This time the tests were carried out with a $7\ m$ long rubber tube, having a diameter of $0.215\ m$ and 1 to $2\ mm$ wall thickness. They were essentially concerned with the measurement of the waves radiated by the tube. Following an extensive series of experiments carried out at Solent University wave tank in Southampton, [7] reports on a linear pneumatic power take-off of adjustable impedance. These tests involved a 1:25 scale model comprising a $7\ m$ long tube, made out of rubber and fabric, with $0.25\ m$ in diameter and held fixed at either end. For the first time, theoretical predictions of power capture were found to be in close agreement with measurements.

Aiming to assess the *Anaconda* performance under intermediate regular waves, in 2014 a 1:100 scale distensible tube model has been coupled at its stern with a forward-bent oscillating water column (OWC) and tested in a wave flume [8]. In this case the $0.81\ m$ long latex tube having a diameter of $7.8\ cm$ floated freely and the OWC model was assembled to a bottom-standing pillar. The pneumatic power take-off used in this experiment had a non-linear pressure to volume flow characteristic that adequately represented an impulse air turbine. The results of this study shed light on various aspects

of the system's response to intermediate water waves and put in evidence the advantages of coupling a distensible tube with an OWC. In this context, a helpful discussion about the problem of a single circular OWC in linear theory is given in [9]. The authors demonstrate that the commercial viability of circular vertical OWCs would require highly efficient power take-off systems; furthermore, in order to have a system capable of harnessing the energy of a large wave front, while delivering a reasonable air flow to the turbine, its optimal capture-width would have to be improved. In light of this the use of a forward-bent duct assembled to a distensible-tube, combined with the use of a reflecting wall, could help to achieve this goal.

The present study reports on experimental tests recently conducted with a 1:70 scale physical model of the OWC-connected distensible tube in a wave flume. The prototype is envisaged to make use of a $60\ m$ long rubber tube, having a diameter of about $7\ m$, operating in water depths of $23\ m$. The periods of the waves generated in the flume scale to $5 - 15\ s$ wave period and up to $5\ m$ maximum wave height, in full-scale. Two situations are modelled: the system operating over a sloping bottom nearshore, or fitted into a reflecting wall onshore. In this later case the system is tested both at constant depth or over the sloped bottom. The dynamic response of the system is obtained from the water column free-surface displacement measurements, in terms of its amplification factor. The air volume-flow across the power take-off is determined by applying Bernoulli's law for incompressible flow, thereafter yielding the extracted power. The energy capture efficiency of the system is then obtained under the form of a capture-width expressed in tube diameters. It is demonstrated that the system is very efficient when allowed to operate with three degrees-of-freedom: in bending, surging and bulging modes. Additionally, it is shown that its performance may be improved by incorporating the proposed onshore configuration.

2. The physical model

A physical model of the OWC-connected distensible tube has been built and tested in a wave flume at a scale of approximately 1:70. The $8\ m$ long and $0.3\ m$ wide flume is equipped with a paddle-type wavemaker and a sloping beach $1.28\ m$ in length at the opposite end. The water depth in the flume is $h = 0.33\ m$. The $0.904\ m$ long tube is made out of $0.16\ mm$ thick latex, and its bow is closed by a wood nose floating head to waves. At its stern the tube is connected to an acrylic vertical circular duct of radius $r = 3.61\ cm$, at a depth of $1.9\ cm$, through a partially submerged PVC elbow. The nose of the tube is itself connected to a water feeding system by means of a $2.5\ mm$ diameter plastic hose, with a tap that pierces the nose. A self-priming reversible flow water pump is used, enabling not only to inflate but also to deflate the rubber tube. The pump can deliver a volume flow of $0.6\ l/min$. By properly adjusting the water head h_0 inside the duct just a few centimetres above the still-water level outside, the rubber tube can be pressurised at will and therefore conveniently tuned to the incident waves. In the present case it is set to $h_0 = 10\ cm$ which results in a pressurized tube diameter $d = 9.78\ cm$. A loose mooring system is also attached to the nose of the tube. The pneumatic power take-off (PTO) consists of an air chamber of height $h_1 = 57.5\ cm$ that connects to the atmosphere through a sharp-edged orifice plate of diameter d_0. The pressure in the

chamber builds under the action of the water piston inside the duct, forcing the air in and out through the orifice. Several calibrated orifices have been tested, with diameters ranging from $d_0 = 5.4\,mm$ to $17.2\,mm$. The model was first tested in the nearshore configuration of Fig. 1, over a 30.1% sloped bottom. Afterwards it was tested on a reflecting wall over constant depth and over the sloping bottom. In Tables 1 and 2 the relevant dimensions of the physical model and PTO system are presented.

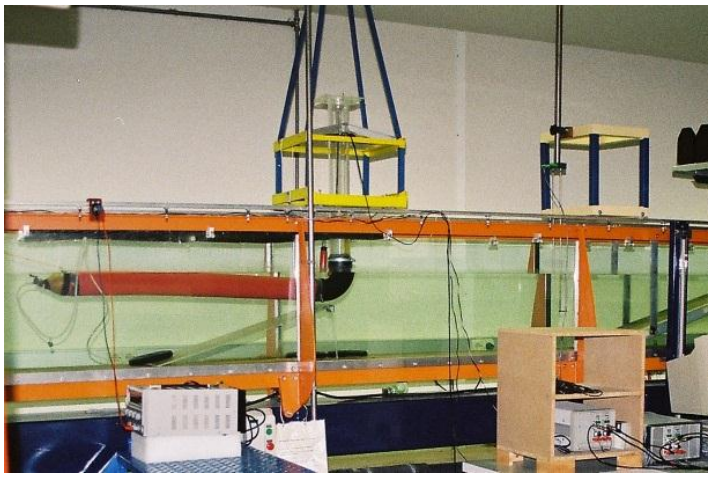

Figure 1: Distensible-tube wave attenuator over a sloping bottom in the wave-flume.

Table 1: Dimensions of the distensible tube at model scale.

Tube length $L\ (cm)$	**Tube diameter** $d\ (cm)$	**Wall thickness** $w\ (mm)$	**Pressure head** $h_0\ (cm)$
90.4	9.78	0.16	10

Table 2: Dimensions of the oscillating water column and PTO at model scale.

OWC diameter $2r\ (cm)$	**OWC length** $l\ (cm)$	**Chamber height** $h_1\ (cm)$	**Orifices diameter** $d_0\ (mm)$
7.22	15.2	57.5	5.4 – 17.2

3. Wave generation and data-acquisition

The wave generator is a bottom-hinged paddle which is driven by a DC electrical motor with controllable speed. Its eccentric disk had to be modified in order to generate very small amplitude waves with a minimum wave height of $1\,mm$, as well as finite amplitude waves up to $80\,mm$ wave height. The wave frequency bandwidth imposed is $0.54 - 1.82\,Hz$. The wave flume and physical model are equipped with four water

level sensors that allow for measurements of wave height upstream and downstream of the model when needed, as well as of OWC free-surface displacement $z(t)$. The measurement uncertainty of these probes is $\pm 0.5\,mm$. Two of them are positioned between the wave generator and the physical model and one is positioned behind, towards the beach. The fourth probe is placed along the axis of the vertical duct. All probes are controlled by a four-channel HR wave-probe monitoring system from Wallingford. The output signals from the 4 water level probes have been logged at $200\,Hz$ for $15\,s$, by a KUSB-3100 S data acquisition card from Keithley and stored on disk. The wave field upstream of the model is equally surveyed with the help of a digital RT oscilloscope TDS220, from Tektronix. A PC 64-bit Pentium Dual-Core CPU E5700 at 3 GHz with 4 GB RAM deals with the data processing. Testpoint V7 is used for data acquisition, instrument control and analysis. In order to determine the incident wave field a reflection analysis algorithm is used to separate the incident and reflected waves [10]. The results presented herein are derived from the fundamental components of the measured wave height and OWC surface elevation records, extracted by Fourier analysis.

In real sea conditions the prototype device is expected to cope with sea waves of roughly 5 to 12 s wave period and up to 5 m wave height. This scales down at 1:70 to waves of $T = 0.6 - 1.4\,s$ and H up to 7.1 cm wave height. A total of six series of regular waves of nondimensional wavenumber $kh = 0.67 - 4.38$ have been generated in the flume. They cover a range of wave periods $T = 0.56 - 1.85\,s$ and wavelengths $\lambda = 0.47 - 3.11\,m$, in water of finite depth $h = 0.33\,m$. Table 3 details the ranges of wave period T, wavenumber k, wave height H and wave celerity c, together with incident wave power P_i which is taken to be the average energy-flux of the incident waves per unit wave crest. In water of finite depth h:

$$P_i = \frac{\rho_1 g H^2 \lambda}{8T} \frac{1}{2} \left(1 + \frac{2kh}{sinh(2kh)}\right) \tag{1}$$

In this expression H is the wave height, λ the wavelength, T the wave period, ρ_1 the mass density of water and k is the fundamental wave number. Wave series 1 and 2 correspond to small amplitude waves having $kH < 0.2$, while wave series 3 to 6 have finite amplitudes for periods roughly bellow $T = 1\,s$.

Table 3: Incident wave-fields generated at model scale.

Wave series	T (s)	k (m^{-1})	H (cm)	c (m/s)	P_i (W/m)
1	0.56 – 1.85	2.02 – 12.76	0.3 – 1.4	0.878 – 1.668	0.020 – 0.099
2	0.56 – 1.85	2.02 – 12.72	0.5 – 2.9	0.880 – 1.665	0.051 – 0.447
3	0.57 – 1.76	2.14 – 12.55	1.4 – 4.5	0.869 – 1.672	0.297 – 1.078
4	0.56 – 1.74	2.17 – 12.84	3.2 – 6.1	0.863 – 1.672	1.169 – 3.002
5	0.55 – 1.85	2.02 – 13.25	3.7 – 7.1	0.862 – 1.671	1.272 – 3.919
6	0.55 – 1.73	2.19-13.27	4.6 – 6.6	0.866 – 1.667	1.817 – 5.284

4. Tuning the model to the incident waves

The system's working principle makes use of the wave-excited pressure bulges in a distensible tube, which thereafter activate OWC oscillations of amplitude η in a forward bent duct. In the present case these periodic water oscillations are utilized to extract useful power by means of a pneumatic power take-off of adjustable impedance. The intensity of the bulges grows along the length of the tube towards the inlet of the duct and is dependent on the incident wave frequency. It has been demonstrated in [4] that resonant conditions may be achieved in the tube if the celerity of the incident waves equals the speed of the pressure bulges. In practice the tuning of a distensible tube can be met by choosing the appropriate material, tube diameter and wall thickness.

As given in [11] the bulge wave speed U inside the rubber tube is $U = 1/\sqrt{\rho_1 D}$, in the absence of hysteresis, where D is the distensibility of the tube. For a tube with circular cross-section of diameter d and wall-thickness w, $D = d/(wE)$; E is the Young's modulus of the tube material, which for latex at 100% strain is $E = 0.91\ MPa$. Hence, the free bulge-wave speed inside the tube is given by $U = \sqrt{wE/\rho_1 d}$. Now, as already mentioned the tuning of the system occurs when the speed of the longitudinal waves in the tube matches the celerity of the surface waves c outside. For $U = c$ the thickness of the tube must then be $w = \rho_1 c^2 d/E$, where $c = (gT/2\pi)\ tanh(kh)$ is the phase velocity of the incident waves in a water depth h. For the present physical model, whose tube dimensions are given in table 1, the expected free bulge-wave speed in the tube is $U = 1.22\ m\ /\ s$ and the corresponding bulge-wave tuning period to be met by the incident surface waves is $T_1 = 0.81\ s$.

Considering next harmonic oscillations of the water column inside the vertical duct, in the absence of the tube, a first approximation the OWC undamped natural period is $T_0 = 2\pi\sqrt{l/g}$. Here l is the length of the water column, measured from the inlet of the PVC elbow till the OWC free-surface. l being currently $15.2\ cm$, $T_0 = 0.78\ s$. In Fig. 2 both the OWC natural period T_0 and the tube's tuning T_1 are represented, for the range of incident wave periods tested. As can be seen, the tube's tuning period is in this case quite close to the OWC natural period. In full-scale, an OWC-connected distensible tube with $d = 6.85\ m$ and $l = 10.64\ m$ will become resonant with incident waves having a period $T = 6.5 - 6.8\ s$. This corresponds to incident wavelengths between $65\ m$ and $70\ m$.

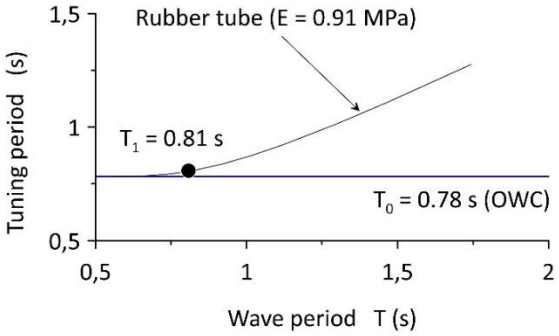

Figure 2: OWC natural period T_0 and tube tuning period T_1 as a function of incident wave period T, for $h = 0.33\ m$.

5. Amplification factor

Aiming to get a response that is as much as possible independent from the influence of the wave flume, an amplification factor ζ has been determined as a function of wave period. This factor is defined as the ratio between the mean water column oscillation height 2η and the incident wave height H. It is represented in Fig. 3 for the system operating nearshore over a sloped bottom. The water-column oscillation height reaches a maximum of 5.6 times the incident wave height near where the incident wavelength is twice the tube's length ($\lambda = 2L$), under the small amplitude waves of series 1. In essence, in order to achieve an amplification factor between 3 and 6 times the incident wave height, a prototype of this device would require a 63 m long tube operating under waves of period $T = 10\ s$, which corresponds to an incident wavelength of about $126\ m$. Note that the typical values of maximum amplification factor for OWCs without a distensible tube lie between 2 to 4.

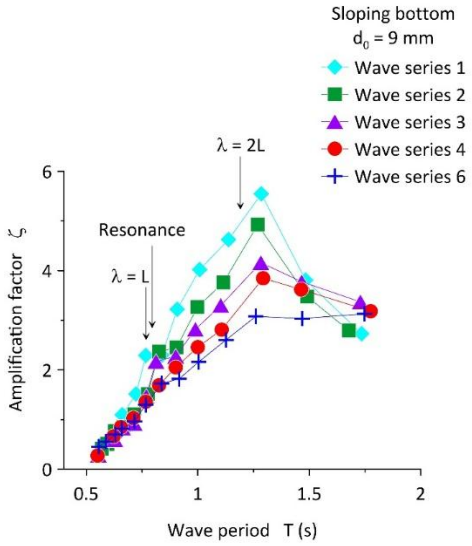

Figure 3: Amplification factor ζ as a function of the incident wave period T, for the nearshore system over a sloping bottom.

6. Pneumatic PTO characteristic

In the present experiment the pneumatic PTO consists of an air chamber which is connected to the atmosphere through a sharp-edged orifice of diameter d_0, bored in a $5\,mm$ thick plate. The air chamber is cylindrical, with cross-sectional area $A = 40.94\,cm^2$ and height $h_1 = 57.5\,cm$, measured from the still water level inside the vertical duct till the orifice. Let V be the volume of air entrapped in the control volume of the pneumatic chamber represented in Fig. 4, which is $V = 2.354\,dm^3$ in this case, and ρ its mass-density at ambient temperature. The corresponding mass of air in the chamber is $m = \rho V$, with $\rho = \rho(p)$ at constant temperature. The decrement in volume caused by a small rise of the water free surface *sl* is $dV = -Adz$ and, neglecting compressibility, the corresponding rate of change of air mass displaced by the water piston will be:

$$\frac{dm}{dt} = -A\rho\frac{dz}{dt} \tag{2}$$

By continuity, the rate of change of mass in the control volume $dm\,/\,dt$ equals the symmetric of the mass flow rate through the orifice. Taking A_0 as the cross-sectional area of the *Vena-contracta*, where the velocity is $v(t)$ toward the atmosphere, we extract from eq. (2):

$$\mathrm{v}(t) = \frac{A}{A_0}\,\frac{dz}{dt} \tag{3}$$

For incompressible conditions the volume-flow rate of air across the orifice is then simply $Q = A(dz/dt)$, where dz/dt is the measured water free-surface velocity in the vertical duct.

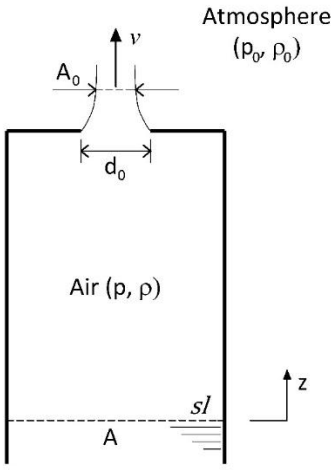

Figure 4: Control Volume of the pneumatic chamber.

If we now apply Bernoulli's law for steady incompressible flow along a streamline exiting from the Control Volume of the pneumatic chamber, the pressure drop Δp across the orifice is:

$$\Delta p = k_0 \frac{1}{2} \rho v^2 \tag{4}$$

where $\Delta p = |p - p_0|$ is the pressure difference between the chamber and the atmosphere, k_0 is the local loss-coefficient and v is the mean flow velocity at the *Vena-contracta*. Assuming a small orifice ($A_0/A \ll 1$), the velocity of the flow in the jet is given by the following expression:

$$v = \pm \frac{1}{\sqrt{1 + k_0}} \sqrt{\frac{2\,\Delta p}{\rho}} \tag{5}$$

Here the factor $1/\sqrt{1 + k_0}$ is the so-called velocity coefficient, which considers the local resistance to the flow. Recall that p is the pressure in the pneumatic chamber, p_0 is the ambient pressure outside and that uniform flow across the *Vena-contracta* has been assumed.

Based on the air velocity given by eq. 5, the volume flow Q through an orifice of diameter d_0 takes the form:

$$Q = C\, \frac{\pi d_0^2}{4} \sqrt{\frac{2\,\Delta p}{\rho}} \tag{6}$$

In this equation $C = \varepsilon/\sqrt{1 + k_0}$ is a discharge coefficient, where ε is the ratio between the section areas of the *Vena-contracta* and the orifice. The pressure to volume-flow characteristic of the present PTO can finally be derived from this last expression and written as follows:

$$\Delta p = KQ^2, \text{ where } K = \frac{8\rho}{C^2 \pi^2 d_0^4} \tag{7}$$

The constant K is known as the orifice characteristic. Given the assumptions stated above, a reasonable empirical value for the discharge coefficient of a small hole in a plate is $C = 0.6$, thus resulting in a value of $K = 2.53 d_0^{-4}$ for ambient air at $945\ mbar$ and $20\ ℃$.

In Fig. 5 a PTO characteristic curve has been derived from the fundamental component of displacement measurements $z(t)$, using eq. 7 with $C = 0.6$. It corresponds to the system shown in Fig. 1 with an orifice with diameter $d_0 = 9\ mm$ and all the wave series tested. For a mean volume-flow rate between 0 and $61\ l/min$ the pressure in the pneumatic chamber rises to about $497\ Pa$, following a typical impulse turbine characteristic.

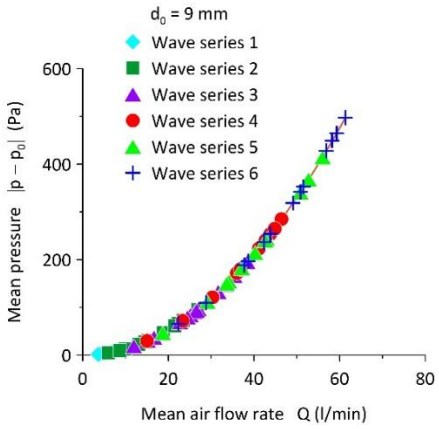

Figure 5: Pressure to volume-flow characteristic of the power take-off system.

7. Extracted power and capture-width

The instantaneous power extracted at the orifice is given in adiabatic conditions by the air flowrate across the orifice $Q(t)$ times the differential pressure $\Delta p(t)$. Hence, the mean power P extracted by the system at each stroke with period T is:

$$P = \frac{1}{T}\int_0^T |\Delta p(t)| \cdot |Q(t)|\, dt \tag{8}$$

Based on the values obtained for the mean extracted power P and the incident wave power per unit wave front P_i, a suitable measure of the system's efficiency is the well-known energy capture-width C_W. It may be defined in tube diameters as follows:

$$C_W = \frac{P}{P_i d} \tag{9}$$

Depicted in fig 6 is the capture-width C_W of the system operating nearshore, with a PTO orifice of diameter $d_0 = 9\ mm$, as a function of wave period T. Out of all the different orifice diameters tested in order to search for a near-optimal PTO impedance rate, the orifice with $d_0 = 9\ mm$ yielded the best energy capture efficiency. The capture-width C_W attains a maximum of 1.78 tube diameters at resonance under waves of series 3. Except for the waves of series 1, whose maximum C_W occurs where $\lambda = 2L$, the peak efficiency happens at resonance near where $\lambda = L$. Here the tube oscillates with a third mode of bending – see Fig. 7. Actually, the small amplitude waves of series 1 are unable to excite this bending mode and thus the capture-width remains under 1 tube diameter at $T = 0.8\ s$. As expected, for waves with significant wave height the effects of the sloping bottom are more important for larger wavelengths, where the waves are influenced by the water depth, contributing to raise the capture-width C_W when $\lambda = 2L$. It is found that the coupling between the bulges in the tube and its bending modes is important, especially at the period where the incident wavelength is equal to the tube length ($T = 0.77\ s$), quite close in this case to T_0 and T_1. This is indeed a determining factor of the system's maximum efficiency. Equally important is the period where $\lambda = 2L$, as confirmed by the amplification factor ζ (Fig. 3).

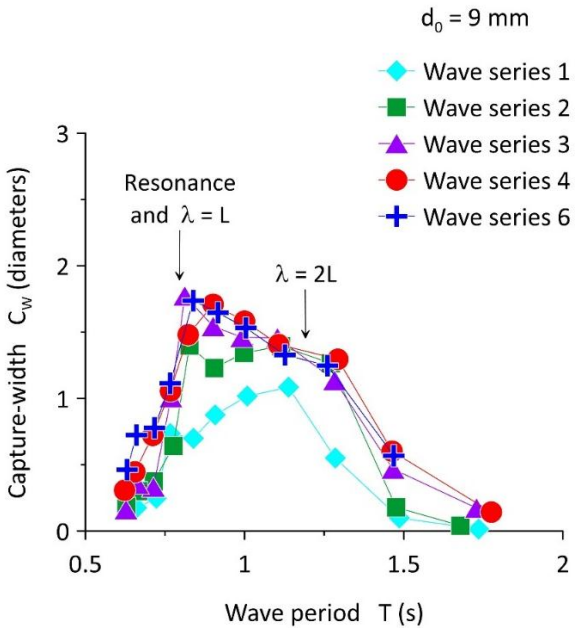

Figure 6: Capture-width C_W as a function of incident wave period T, for the model over a sloping bottom with a PTO orifice of diameter $d_0 = 9\ mm$.

Figure 7: Tube's fully developed third-mode of bending.

8. Onshore system in a sea-wall

Fig. 8 represents the distensible tube system fitted into a reflecting barrier. This model enables to test the system in the onshore configuration in water of variable or constant depth and compare the results with the nearshore configuration of Fig. 1.

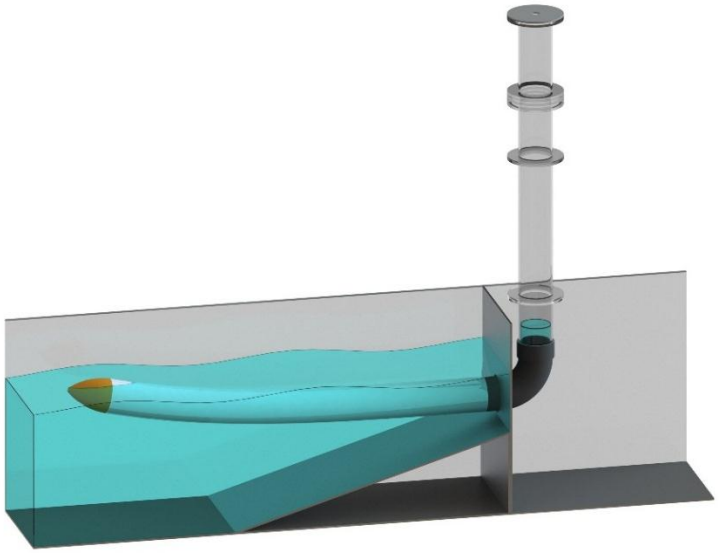

Figure 8: Distensible-tube wave attenuator fitted into a reflecting wall over a 30.1% slope removable bottom.

A comprehensive comparison is made between the nearshore and onshore situations previously studied, whose energy capture efficiency is consolidated in fig. 9 for wave series 1, 2, 4 and 6. In terms of capture-width neither the water-depth variation nor the inclusion of a reflecting barrier bring foreseeable efficiency improvements bellow $T \approx 0.77\ s$. Above this period the barrier at constant water-depth leads to an increase in maximum capture-width of at most 28% relative to the nearshore system on a sloped bottom, for the highly energetic waves of series 4 and 6. The system fitted on a sea-wall over a sloping bottom is capable of attaining an even higher maximum capture-width, reaching 2.26 tube diameters at $T = 1\ s$ for the waves of series 6. The influence of a sloping bottom is twofold: on one hand it amplifies the height of the incident waves as they travel along the tube towards the barrier; on the other hand it gives rise to a second mode of bending of the tube when $\lambda = 2L$, which increases the bandwidth of high capture-width. The bending modes at $\lambda = L$ and $\lambda = 2L$ are relevant in determining not only the peak efficiency, but also the bandwidth where $C_W > 1$. It is worth noting that the barrier over constant depth is unable to excite the bending mode at $\lambda = 2L$ for the small amplitude waves of series 1 and 2. All these considerations become pivotal when designing a nearshore or onshore application.

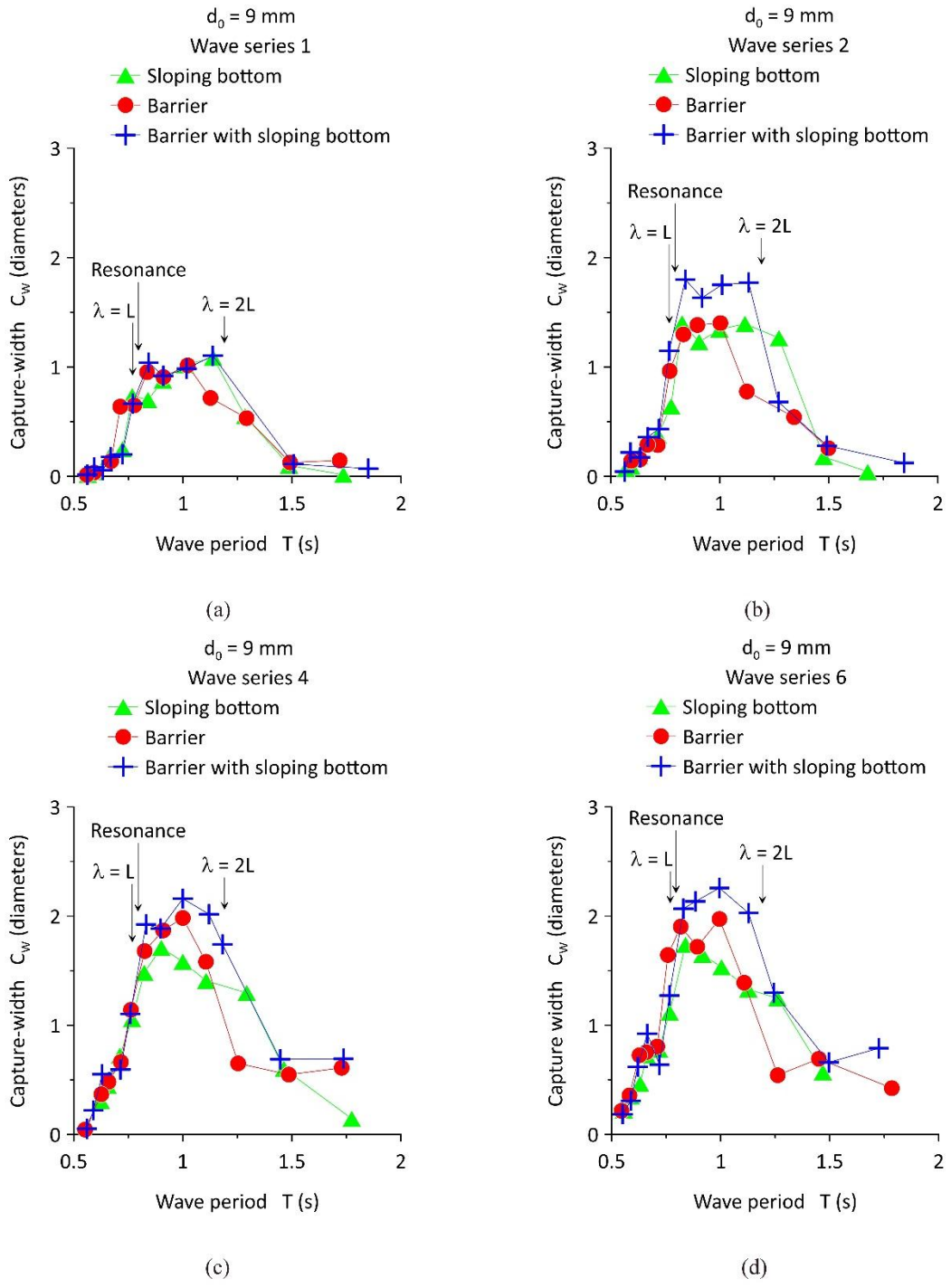

Figure 9: Capture-width C_W versus wave period T for the nearshore and onshore configurations studied under wave series 1 (a), wave series 2 (b), wave series 4 (c) and wave series 6 (d).

9. Hydrodynamic and overall efficiencies

An energy balance which comprehends a far-field analysis of the reflected and transmitted waves, together with the extracted power at the PTO is now accomplished. The wave measurements have been performed sufficiently far from the model so that evanescent modes had decayed. Part of the incident wave energy is transferred to the system at its primary interface, with the remaining fraction being reflected and transmitted by the tube oscillations or lost due to viscosity. A reflection analysis of the waves upstream yields the total reflection coefficient R and the transmission coefficient T_r is monitored by the wave probe downstream of the model. The system's hydrodynamic efficiency is then $1 - R^2 - T_r^2$. In order to complement the performance assessment of the system, an overall efficiency is also defined as the ratio of the extracted energy PT to the incident wave energy over the width of the flume. Fig. 10 gathers these two efficiencies as a function of the incident wave period for the onshore system in a sea wall over a sloping bottom of Fig 8. The hydrodynamic efficiency is maximum at resonance ($T = 0.81\ s$), almost reaching 1, and falls dramatically as the wave period increases. It is known that the energy losses are larger for waves of small periods, decreasing monotonously as the wave period increases. As a consequence, the overall efficiency attains a maximum of 0.48 between $T = 0.81\ s$ and $T = 1\ s$. In practice the system extracts at most 48% of the total wave power available in a wave front equal to the flume width. For wave periods under the system's resonance the hydrodynamic efficiency is very high and the overall efficiency is poor. This difference reflects a surplus of energy which is not converted into useful power, in part due to wave breaking over the nose and on top of the tube (see Fig. 11) as well due to other energy dissipation mechanisms.

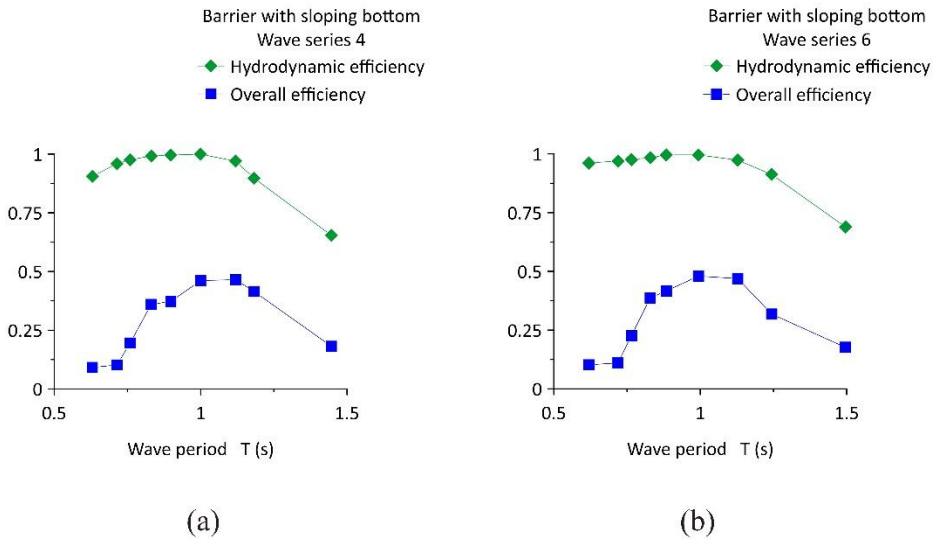

Figure 10: Hydrodynamic and overall efficiencies of the system fitted on a sea-wall over a sloping bottom, as a function of wave period T, obtained with an orifice of diameter $d_0 = 9\ mm$ under wave series 4 (a) and wave series 6 (b).

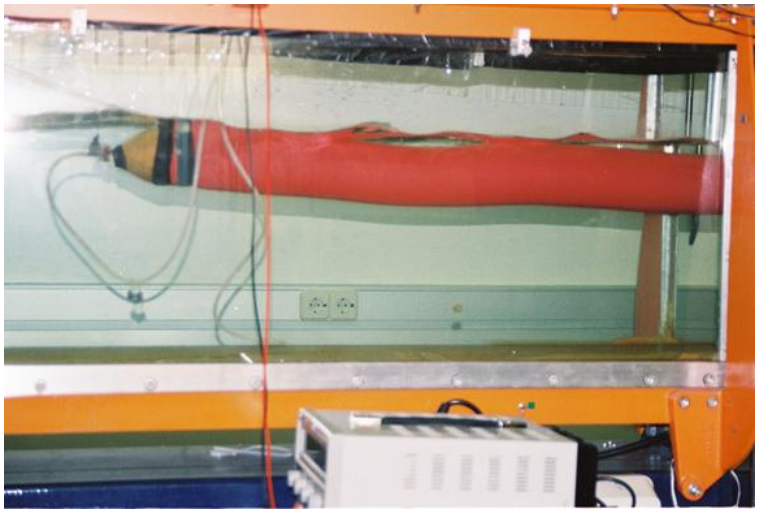

Figure 11: Interference of the incident waves with the tube and flume side-walls.

10. Summary and conclusions

The present research focuses on the performance assessment of a simple and low-cost device which can be deployed at the nearshore or onshore, incorporating well-tried rubber and turbine technologies. To that end a 1:70 scale model of an OWC-connected water filled distensible tube has been tested in a wave flume, freely floating head to regular waves. Air compressibility has been neglected, an assumption that is to some extent valid for small-scale laboratory work. A total of sixty waves per PTO impedance have been generated in the wave flume that correspond to the envisaged nearshore wave conditions. In each wave series 23% were deep water waves and 77% were intermediate waves. In full-scale they translate to waves with periods from 4.6 s to 15.5 s and up to 5 m wave height.

A prototype of the device is foreseen to utilize a rubber tube roughly 63 m long with about 7 m in diameter. The bulge-wave tuning period scales to 6.8 s, which corresponds to waves having a wavelength of about 70 m propagating in a water depth of 23 m. Coincidently, the natural frequency of the oscillating water column is at 6.5 s. Moreover, when the incident waves have a wavelength twice the length of the tube, i.e. about 126 m, a resonant bending mode is also apparent which proves to be beneficial for wave energy extraction. The maximum energy capture-width attained is 2.26 tube diameters for the most energetic waves and it occurs close to the tube tuning, for the onshore configuration. For the nearshore configuration it does not exceed 2. Under these conditions the tube oscillates with an extra surging motion, apart from significant bending and bulging. When operating near the tube tuning under waves of 3.5 m wave height, the onshore system is then able to capture the energy of a 15.5 m long wave front in average. When under waves of smaller wave height, of the order of 0.5 m, the tube is instead sensitive to wavelengths of about 126 m, which is twice the length of the tube in full-scale. In general, the system is efficient ($C_W > 1$) for a large range of sea waves with periods roughly between 6 s and 11 s. The effect of a sloping bottom

is beneficial and results in tube bending modes which also resonate when $\lambda = 2L$. A relevant aspect is that the onshore system fitted in a sea wall, over a sloping bottom, responds efficiently not only to waves with wavelength of the order of two times the tube length but also in resonant conditions.

Acknowledgments

The present research was conducted in the Laboratory of Fluid Mechanics and Turbomachinery at Universidade da Beira Interior, in Portugal. The work was partially funded by The Portuguese Foundation for Science and Technology and The European Union. The authors are grateful to the Emeritus Professor John Chaplin (University of Southampton) for sharing his expertise on the subject. The skills and goodwill of Mr. Morgado demonstrated during the manufacture of the physical model are also acknowledged.

References

[1] World Energy Council, 2016, "World Energy Resources – Marine Energy", London. [Online] Available: http://large.stanford.edu/courses/2018/ph240/rogers2/docs/wec-2016.pdf

[2] Foley, M. and Whittaker, T. J. R., 2009, "Analysis of the Nearshore Wave Energy Resource", Renew. Energy, 34, pp. 1709-1715. DOI:10.1016/j.renene.2009.01.003

[3] Farley, F. J. M. and Rainey, R. C. T., 2006, "Distensible Tube Wave Energy Converter", British patent N. GB 2434840, UK Intellectual Property Office.

[4] Chaplin, J. R., Farley, F. J. M. and Rainey, R. C. T., 2007, "Power Conversion in the Anaconda WEC", in Proc. of the International Workshop on Water Waves and Floating Bodies, 4 pp., Plitvice.

[5] Chaplin, J. R., Farley, F. J. M., Prentice, M. E., Rainey, R. C. T., Rimmer, S. J. and Roach, A. T., 2007, "Development of the Anaconda All-Rubber WEC", in Proc. of the 7th European Wave and Tidal Conference, Ed. A. F. Falcão et al., 13 pp., Porto.

[6] Chaplin, J. R., Farley, F. J. M., Hearn, G. E., Heller, V. and Mendes, A., 2010, "Hydrodynamic Performance of the Anaconda Wavepower Device", in Proc. of the HYDRALAB III Closing Event, Hannover.

[7] Chaplin, J. R., Heller, V., Farley, F. J. M., Hearn, G. E. and Rainey, R. C. T., 2012, "Laboratory Testing the Anaconda", Philos. Trans. Royal Soc. A, 370, pp. 403-424. DOI:10.1098/rsta.2011.0256

[8] Mendes, A. C., Paredes, L. M. A., Gil, F. A. S. and Chaplin, J. R., 2014, "Small-Scale Model Tests of a Rubber-Tube Wave Energy Converter with Pneumatic Power Take-Off", in Proc. of the ASME 33rd International Conference on Ocean, Offshore and Arctic Engineering, San Francisco. DOI:10.1115/OMAE2014-23452

[9] Evans, D. V. and Porter, R., 1997, "Efficient Calculation of Hydrodynamic Properties of OWC-Type Devices", J. Offshore Mech. Arct. Eng., 119(4), pp. 210-218. DOI:10.1115/1.2829098
[10] den Boer, K., 1981, "Estimation of Incident and Reflected Wave Characteristics of Perpendicular Wave Action", Research report S 434, Vol. I, Delft Hydraulics Laboratory, The Netherlands.
[11] Lighthill, J., 1978, "Waves in Fluids", Cambridge University Press, Cambridge.

Biographical sketch

António C. Mendes, Associate Professor with tenure (now Jubilated). Professor of Fluid Mechanics and former head of the laboratory of Fluid Mechanics and Turbomachinery at Universidade da Beira Interior, Portugal. Member of ASME – Ocean, Offshore and Arctic Engineering Division. Editorial Board Member of The International Journal of Dynamics of Fluids.

Francisco P. Braga, Msc. Research Assistant of Fluid Mechanics at the Electromechanical Engineering Department of Universidade da Beira Interior in Portugal.